
Article:
Utton, C.A., Papadimitriou, I., Kinoshita, H. et al. (2017) Experimental and thermodynamic assessment of the Ge-Nb-Si ternary phase diagram. Journal of Alloys and Compounds, 717. pp. 303-316. ISSN: 0925-8388

https://doi.org/10.1016/j.jallcom.2017.04.279

Experimental and thermodynamic assessment of the Ge-Nb-Si ternary phase diagram

Claire A Utton[a] *, Ioannis Papadimitriou[a], Hajime Kinoshita[a], Panos Tsakiropoulos[a]

[a] Department of Materials Science and Engineering, The University of Sheffield, Sir Robert Hadfield Building, Mappin Street, Sheffield S1 3JD, England, UK

Abstract

Niobium silicide-based in-situ composites have the potential to supersede nickel-based superalloys due to their excellent high temperature mechanical properties and low density. The addition of small amounts of germanium into these systems can significantly improve oxidation resistance. The effect of germanium on the phases formed in bulk niobium silicide-based in-situ composites is not particularly well understood, in particular the effect of introducing germanium on the formation of the Nb_5Si_3 intermetallic. Limited data is available in the literature. To provide coherent information on the effect of germanium on the phase equilibrium in the Nb-Si system, a comprehensive thermodynamic description of the Ge-Nb-Si system has been developed in the current paper using the CALPHAD method. Initially the Ge-Nb phase diagram was reassessed using the CALPHAD method to take into account recent ab initio data. To supplement limited information on the ternary system in the literature between 800-1820°C, the pseudo binary between Nb_5Si_3 and Nb_5Ge_3 was studied experimentally between 1200-1500 °C. Experimental and modelling results indicate that the W_5Si_3 prototype of Nb_5Si_3 can be stabilised to lower temperatures on the addition of germanium. Ge contents in excess of 12.4 at. % at 1200°C in stoichiometric $Nb_5(Ge,Si)_3$ stabilise the W_5Si_3 prototype. In non-stoichiometric $Nb_5(Ge,Si)_3$, where Nb < 62.5 at. %, lower amounts of Ge are required to stabilised the W_5Si_3 prototype. The liquidus projection suggests a ternary eutectic with $Nb_5(Ge,Si)_3$, Nb_{ss} and Nb_3Si can form in Nb-Si rich alloys during solidification.

Key words: Ge-Nb-Si, Niobium silicides, germanium, CALPHAD, thermodynamics, phase diagrams

Highlights

- The Ge-Nb phase diagram has been reassessed
- A thermodynamic assessment for Ge-Nb-Si is presented
- Calculated phase diagrams agree well with experimental data
- The addition of germanium is shown to stabilise the W_5Si_3 prototype of Nb_5Si_3 to low temperatures
- Liquidus and Scheil indicate a ternary eutectic (Nb-Nb_5Si_3-Nb_3Si) will likely be present in Nb-Si rich alloys with Ge.

1.0 Introduction

Significant efforts have been made world-wide in the last 5 decades to improve reliability, extend life times and importantly to reduce the environmental impact of aerospace gas turbine engines. To reduce the environmental impact and improve the efficiency and performance of gas turbine engines, greater fuel efficiency and a reduction in the weight is required. This can most notably be achieved by increasing the combustion temperature of the fuel in the engine, and/or by reducing the airfoil mass. The most advanced Ni-based superalloys currently used in gas turbine engines are

*Corresponding author at: Department of Materials Science and Engineering, The University of Sheffield, Sir Robert Hadfield Building, Mappin Street, Sheffield S1 3JD, England, UK

email address: c.utton@sheffield.ac.uk (C.A.Utton)

reaching the limit of their temperature capabilities, and as such increases in fuel combustion temperatures are limited. These alloys are currently operating at surface temperatures around 1150 °C in their hottest areas whilst their melting occurs at around 1350 °C. Thus, there is need for new high temperature refractory alloys in order for the gas turbine technology to advance.

Niobium silicide-based alloys, which consist of Nb solid solution (Nb_{ss}) with Nb_5Si_3 and/or Nb_3Si intermetallics, are good candidate materials for these high temperature applications. They have desirable mechanical properties at both low and high temperatures and low density [1]. Introduction of germanium into these systems is particularly interesting as it can improve their oxidation resistance [2]. Germanium is reported to benefit high temperature oxidation resistance of coatings used on refractory silicide alloys. During oxidation a glassy $GeO_2.SiO_2$ phase develops which fills cracks and is impermeable to further oxygen penetration [3]. The addition of germanium to bulk niobium silicide-based alloys is reported to improve oxidation resistance at both high and low temperatures [2,4]. Germanium in synergy with boron has also been shown to improve the oxidation resistance at 1200-1250 °C. On the addition of 5 at. % Ge with 4 at. % B to the alloy Nb-24Ti-15Si-13Cr-2Al-2Hf a nearly 5-fold reduction was measured in weight gain during oxidation [5].

However, the application the Nb-Silicide based alloys containing additions such as Ge is still restricted because of the limited understanding of the Ge-Nb-Si system, in particular the effect of introducing Ge on the formation of the Nb_5Si_3 intermetallic. The stable intermetallic is important to establish as it can determine subsequent phase transformations (e.g. Nb_3Si eutectoid decomposition) and mechanical properties (e.g. the coefficient of thermal expansion of βNb_5Si_3 is more anisotropic than αNb_5Si_3). Approximately 5 at. % of Ge inclusion was reported to stabilise βNb_5Si_3 over αNb_5Si_3 in complex multi component alloys e.g., Nb-19.9Ti -19.7Si-4.2Ge-3.3Al-4.2Hf-9.9Cr and Nb-26.0Ti-12.6Si-4.9Ge-1.9Al-1.9Hf-6.7Cr-0.43Sn after heat treatment at 1200°C [6]. The phase αNb_5Si_3 was observed in samples containing no Ge [6]. More recently Li and Tsakiropoulos [7] studied two alloys (ZF1 Nb-18Si-5Ge and ZF2 Nb-18Si-10Ge) at 1200°C and 1500°C to understand the effect of Ge on phase stability and microstructure. Samples were argon arc melted and analysed using bulk X-ray diffraction (XRD) analysis, scanning electron microscopy (SEM)/electron dispersive spectroscopy (EDS) and micro hardness. In the as-cast (AC) microstructure Nb_{ss} and βNb_5Si_3 were identified for both alloys. Primary βNb_5Si_3 formed, followed by Nb_{ss} and a fine eutectic of Nb_{ss} and βNb_5Si_3. However, after heat treatment for 100h at 1200°C and 1500°C under argon, the authors observed the transformation of βNb_5Si_3 to αNb_5Si_3. The authors also measured the micro hardness of the alloys and observed that the hardness increased with increasing Ge content and the hardness of both alloys increased significantly after heat treatment at 1500°C.

Although the overall effect of Ge appears to be positive, to the authors knowledge no coherent information is currently available in the literature on the effect of Ge on the temperature stability range of the Nb_5Si_3 and its effect on the microstructural properties.

To provide coherent information on the effect of Ge on the phase equilibria in the Nb-Si system, a comprehensive thermodynamic description of the Ge-Nb- Si system has been developed in the current paper using the CALPHAD method. In this paper the pseudo binary between Nb_5Si_3 and Nb_5Ge_3 has been studied experimentally between 1200-1500 °C, to supplement limited information on the ternary system in the literature between 800-1800°C. A thermodynamic description for the ternary system was developed by extrapolation of thermodynamic descriptions of binary systems (Ge-Si, Ge-Nb and Nb-Si) and optimisation using newly obtained data and previously published work. The thermodynamic description of the Ge-Nb binary phase diagram was modified to take into account recent ab initio data [8]. This paper presents the experimental data obtained along the pseudo binary and the outcomes of thermodynamic modelling. Using the developed thermodynamic description, the Ge-Nb-Si ternary isotherm has been obtained at different temperatures, and the

effect of Ge on the phase equilibria, in particular on the stable temperature range of Nb_5Si_3 is discussed.

2.0 Review of the literature on phase diagrams

2.1 Nb-Si system

As shown in Fig. 1 [9], in the Nb-Si system 4 intermetallic phases are present; Nb_3Si (*tP*32 Ti_3P – type), αNb_5Si_3 (*tI*32 Cr_5B_3 – type), βNb_5Si_3 (*tI*32 W_5Si_3 – type), and $NbSi_2$ (*hP*9 $CrSi_2$ – type), and 2 solid solution phases; Nb (cI2 Im-3m) and Si (cF8 Fd-3m). Nb_5Si_3 has two isomorphs. A low temperature form, αNb_5Si_3, stable from room temperature to 1934 °C and a high temperature form, βNb_5Si_3, observed between 1648 and 2525 °C depending on composition. Both Nb_5Si_3 isomorphs have a tetragonal crystal structure (tI32, I4/mcm) however are based on different prototypes (e.g. they have the same structure but crystallise in different atomic arrangements). The phase βNb_5Si_3 has the W_5Si_3 prototype, whereas αNb_5Si_3 has the Cr_5B_3 prototype. As such the lattice parameters are distinct, and the two phases may be distinguished using XRD. The thermodynamic description for the Nb-Si system has been reported by Geng et al. [9] and is used in the current thermodynamic description.

2.2 Ge-Nb system

The Ge-Nb system was modelled by Geng et al. [10]. The Ge-Nb system contains 3 intermetallic phases; Nb_3Ge (*cP*8 Cr_3Si - type), Nb_5Ge_3 (*tI*32 W_5Si_3 – type), $NbGe_2$ (*hP*9 $CrSi_2$ – type), and 2 solid solution phases; Nb (cI2 Im-3m) and Ge (cF8 Fd-3m) as shown in Fig. 2 [10]. When plotting the diagram using the published dataset a small inadvertent miscibility gap was seen at the Nb_3Ge-liquid phase boundary (Figure 2a – inset). In addition, when merging the data with the Nb-Si binary, the description of a metastable phase in Nb_5Ge_3 ($Nb_{0.5}Nb_{0.125}VA_{0.375}$) had an effect on the phase description of βNb_5Si_3 in the Nb-Si binary phase diagram (Figure 1 – inset b).

In the previously reported literature [11-14] there is a conflict over the prototype structure of the Nb_5Ge_3 phase, whether it has the Cr_5B_3 or W_5Si_3 prototype. First principles calculations reported in our previous study using CASTEP [8] indicate that the W_5Si_3 prototype is more stable than the Cr_5B_3 structure, over the whole temperature range (at 0 K by -0.1 kJ/mol atom). However, Colinet et al. [15] recently performed similar calculations using VASP but instead found that the Cr_5B_3 prototype was more stable than the W_5Si_3 prototype (by -0.3 kJ/mol at 0 K). It is suggested that the difference is related to the pseudo potentials used. In this study we are basing the phase diagram on our calculations [8], which appear to be confirmed by the experimental results in the current work (e.g. XRD analysis reported in section 4.0). As such βNb_5Si_3 and Nb_5Ge_3 are considered in this study to be isomorphous, both having the W_5Si_3 prototype.

Another issue in the previously reported diagrams is the uncertainty in the stability of a hexagonal phase, $Nb_{10}Ge_7$ (*hP*16 Mn_5Si_3 – type), also known as Nb_3Ge_2 [11-13, 16-18]. In the following work the hexagonal phase will be referred to as $Nb_{10}Ge_7$. Due to the uncertainty of the stability of this phase, Geng et al. [10] reported two calculated phase diagrams for the Ge-Nb system; one containing the phase $Nb_{10}Ge_7$ and one without (Fig. 2 is based on the latter). Our first principles calculations indicate that this phase should not be stable over the whole temperature range, and is likely metastable or stabilised by impurities [8]. Colinet et al. reports a more negative value for $Nb_{10}Ge_7$, calculated using VASP, however at 0 K this phase is still not stable [15]. As such in the following assessment, $Nb_{10}Ge_7$ is assumed to be metastable and hence not included in the model.

Papadimitriou et al. [8] and Colinet et al. [15] report the enthalpy of formation for the intermetallics at 0 K calculated using first principles. These values are more negative than those used in the CALPHAD assessment by Geng et al. [10], which was fit to the available experimental values.

Minor modifications were made to the thermodynamic description of Nb_3Ge reported by Geng et al. [10]. Geng et al. [10] proposed the sublattice model $(Nb)_3(Ge, Nb, VA)$ where VA represents a vacancy in the sublattice (further explanations provided in the modelling section 5.2.3) to describe the compositional range of Nb_3Ge (18-23 ±1 at. % Ge). First principles calculations showed that the vacancies on the second sublattice were not thermodynamically favoured [8]. Therefore, this binary thermodynamic description has been modified to be $Nb_3(Ge, Nb)$.

To summarise the phase diagram was reoptimised to 1) remove the small inadvertent miscibility gap, 2) modify the metastable phase ($Nb_{0.5}Nb_{0.125}VA_{0.375}$) affecting the Nb-Si phase diagram, 3) to consider recent ab initio results, and 4) accommodate the change in sublattice description.

2.3 Ge-Si system

The parameters for the Ge-Si system are taken from SGTE Solutions Database Version 4.8 (SSOL4) [19]. The calculated phase diagram is shown in Figure 3. The Ge-Si binary system has a solid solution phase of Ge and Si (cF8 Fd-3m) and a liquid phase.

2.4 Ge-Nb-Si system

There is limited information on the ternary Ge-Nb-Si phase diagram. The ternary phase diagram has been studied primarily for the potential application of $Nb_x(Ge,Si)_y$ phases as a super conducting compounds. The Nb-rich corner of the Ge-Nb-Si phase diagram was experimentally studied previously by Pan et al. [20, 21] to establish the influence of Ge on the formation of A15 Nb_3Si. They reported two partial experimental phase diagrams of the Ge-Nb-Si system at 1780 and 1820 °C and an interpolated phase diagram at 1800°C, in which the data was estimated between the two phase diagrams at 1780 and 1820 °C. The phase diagrams at 1780 and 1820 °C have been redrawn by the present authors for clarity and are shown in Fig. 4 [20, 21]. They selected 1780 and 1820 °C because Nb_3Si is stable within this region. In their phase diagrams, no ternary phases are present, but numerous solid solutions are observed (Fig. 4). At 1820 °C, the solubility of Ge in Nb is approximately 8 at. %, whereas the solubility of Si is approximately 1 at. %. Nb_3Ge can accommodate up to 10 at. % Si whereas the solubility of Ge in Nb_3Si is limited to a maximum of 2 at. %. In contrast, the solubility of Si in Nb_5Ge_3 is large, up to approximately 30 at. %. In Nb_5Si_3, Ge solubility is limited to approximately 6 at. %.

The isothermal sections presented by Pan et al. require an update, as additional and more reliable information has become available on the binary phase diagrams since they presented these isothermal sections. The binary Nb-Si phase diagram used in their study is different from the currently established diagram shown in Fig. 1. Pan et al. considered that the eutectoid reaction $Nb_3Si \rightarrow \alpha Nb_5Si_3$ + BCC occurred at approximately 1800°C whereas in the phase diagram presently accepted, Nb_3Si is stable down to 1673°C [9]. In addition, they did not include αNb_5Si_3 which according to the current model should be stable and in equilibrium with βNb_5Si_3 (Fig. 1) at the temperatures they studied.

In the Ge/Si rich regions of the phase diagram the available information is limited. It is reported that $NbGe_2$ and $NbSi_2$ (hP9 $P6_222$) have complete solid solubility [22]. No thermodynamic data on the Nb-Ge-Si ternary system have been reported.

3.0 Experimental

In order to understand the effect of germanium on the stability of Nb_5Si_3 between 800-1600 °C, and provide additional data for modelling the phase diagram, the pseudo binary between Nb_5Si_3 and Nb_5Ge_3 was studied experimentally. Samples were produced with compositions along the stoichiometric pseudo binary between Nb_5Si_3 and Nb_5Ge_3 by substituting the Si content with Ge. Nominal compositions are shown in Table 1.

Samples were made using argon arc melting of pure metals (99.8 wt.% Nb, 99.9999 wt.% Si and 99.999 wt.% Ge) under a high purity argon atmosphere in a copper water-cooled crucible with a non-consumable electrode. Mass losses after arc melting were less than 0.1 wt%. Producing an alloy with a specific composition, in particular a single phase alloy, using arc melting is challenging and it may be expected that the actual composition varies from the nominal composition due to vaporisation or that additional phases may form. Nb_5Ge_3 and βNb_5Si_3 form congruently from the melt and as such their formation using arc melting is simplified.

The arc melted samples (as-cast) were sectioned and selected pieces wrapped in Ta foil and heat treated for 100 hours under flowing argon at either 1200 or 1500°C. The as-cast and heat treated samples were crushed in an agate pestle and mortar and a thin film prepared for transmission XRD analysis. To prepare the film the powder was mixed with water based glue and applied to a zero scattering foil and allow to dry. A STOE STADI P transmission X-ray diffractometer with Cu-Kα radiation was used with measurements over the range 15 and 90° 2-theta. Phase identification was performed using PDF++/Sleve software.

4.0 XRD Results and Discussion

XRD for as-cast and heat treated samples are shown in Figs. 5 and 6. In all as-cast samples a single dominant phase was observed. This phase has the tetragonal tI32 structure with the W_5Si_3 prototype. Both the high temperature stable βNb_5Si_3 and Nb_5Ge_3, have this crystal structure, and it is suggested that they make up two end members of a solid solution range. The major difference between the two phases is that Nb_5Ge_3 is stable from room temperature to its melting temperature, whereas βNb_5Si_3 is stable between 1648°C to 2525°C. It appears that there is a continuous solid solution between these two phases under the conditions in the present study. Hereafter the W_5Si_3 solid solution phase is referred to as $Nb_5(Ge,Si)_3$. As the amount of Ge in $Nb_5(Ge,Si)_3$ increases the reflection peaks for the $Nb_5(Ge,Si)_3$ are shifted to lower angles due to replacement of Si with larger Ge atoms and the subsequent increase in lattice parameters. In the 20 and 30 at. % Ge sample small additional peaks for Nb_3Ge were identified. In the 5 and 10 at. % Ge samples a small broad peak was attributed to Nb_{ss}. Both Nb_3Ge and Nb_{ss} may form during solidification.

After heat treatment at 1200°C, $Nb_5(Ge,Si)_3$ in the 5 and 10 at. % Ge samples transformed to the lower temperature stable phase αNb_5Si_3. In the 15 at. % Ge sample both αNb_5Si_3 and $Nb_5(Ge,Si)_3$ were identified while at 20 and 30 at. % Ge $Nb_5(Ge,Si)_3$ was observed. Small peaks for a secondary phase, likely Nb_3Ge, in the 30 at. % Ge sample were again seen, but not in the 20 at. % Ge sample. The peaks attributed to Nb_{ss} were no longer observed.

After heat treatment at 1500°C, all but the 15 at. % Ge sample had the same stable phases as seen at 1200°C. The 30 at. % Ge sample was not analysed due to severe oxidation during heat treatment. As this sample was well within the single phase $Nb_5(Ge,Si)_3$ region it was not felt significant to repeat. At 15 at. % Ge, αNb_5Si_3 did not form, instead $Nb_5(Ge,Si)_3$ was the only phase observed. This suggests

that at 1500°C this alloy is within a single phase region, compared to the same alloy at 1200°C which was in a two phase region.

5.0 Thermodynamic modelling

5.2.1 Elements

The Gibbs energy of a pure element i (Ge, Nb, Si) in a particular crystal structure as a function of temperature is given by:

$$^{o}G_i^{\varphi} - H_i^{SER} = a + bT + cTln(T) + dT^2 + eT^3 + fT^{-1} \ldots \quad (1)$$

where H_i^{SER} is the molar enthalpy of formation of the element i in its stable reference state at 298.15 K and atmospheric pressure (101325 Pa), T is temperature and a, b, c... etc. are coefficients. The Gibbs energy functions for Nb, Ge and Si have been taken from the Scientific Group Thermodata Europe (STGE) database compiled by Dinsdale [23].

5.2.2 Solution phases

The Gibbs energy of Liquid, Diamond (Si and Ge - cF8 Fd-3m) and BCC (Nb - cI2 Im-3m) phases are described as substitutional solutions. The Gibbs energy per mole of phase is given by the expression below, where φ represents a phase (BCC, Liquid or Diamond) and the notation n indicates that these phases are composed of mixture of elements rather than a single element i. A substitutional solution model was used in the present study, and the excess term is described by the Redlich-Kister equation.

$$G_n^{\varphi} - H_n^{SER} = {}^{ref}G_n^{\varphi} + {}^{id}G_n^{\varphi} + {}^{ex}G_n^{\varphi} \quad (2)$$

$^{ref}G_n^{\varphi}$ is the Gibbs energy contribution of pure elements involved in a phase, $^{id}G_n^{\varphi}$ is the statistical contribution caused by mixing atoms in the ideal solution, and $^{ex}G_n^{\varphi}$ is an excess contribution due to the interaction of atoms, which represent the deviation from the ideal solution. They are expressed as

$$^{ref}G_n^{\varphi} = x_{Ge}\,{}^{o}G_{Ge}^{\varphi}(T) + x_{Nb}\,{}^{o}G_{Nb}^{\varphi}(T) + x_{Si}\,{}^{o}G_{Si}^{\varphi}(T) \quad (3)$$

$$^{id}G_n^{\varphi} = RT(x_{Ge}lnx_{Ge} + x_{Nb}lnx_{Nb} + x_{Si}lnx_{Si}) \quad (4)$$

$$^{ex}G_n^{\varphi} = x_{Ge}x_{Nb}\sum_j {}^{j}L_{Ge,Nb}^{\varphi}(x_{Ge} - x_{Nb})^j + x_{Ge}x_{Si}\sum_j {}^{j}L_{Ge,Si}^{\varphi}(x_{Ge} - x_{Si})^j + x_{Nb}x_{Si}\sum_j {}^{j}L_{Nb,Si}^{\varphi}(x_{Nb} - x_{Si})^j \quad (5)$$

where x_i is the mole fraction of element i, T is temperature and R is the gas constant. The terms in $^{ex}G_n^{\varphi}$ with L e.g. $^{j}L_{Ge,Nb}^{\varphi}$ are binary interaction parameters where j = 0-2. Binary interaction parameters for Nb-Si and Si-Ge were taken directly from the literature, whereas the Nb-Ge parameters were optimised in the present paper. For BCC, Liquid and Diamond phases no ternary excess parameters were used.

5.2.3 Intermetallic phases

Si is soluble in Nb_3Ge and Ge is soluble in Nb_3Si and αNb_5Si_3. βNb_5Si_3 forms a complete solid solution with Nb_5Ge_3, and thus, is considered to be a single $Nb_5(Ge,Si)_3$ phase. Similarly, $NbGe_2$ and $NbSi_2$ have complete solid solubility and are considered as a single $Nb(Ge,Si)_2$ phase. A two-sublattice model was used for the description of all the intermetallic phases, except for $Nb_5(Ge,Si)_3$ where a three-sublattice model was used. The Gibbs energies were described by the (sub-) regular solution model [24].

The two-sublattice model $(\mathbf{Nb})_{0.75}(Ge,\mathbf{Si})_{0.25}$ was used for Nb_3Si. The elements in bold are the major elements in the sublattice. Given the size and similarity of Ge and Si it is reasonable to assume Ge will substitute on the second sublattice only. The Gibbs energy function for Nb_3Si is given by the following equation, where φ = Nb_3Si and ${}^{j}L$ is the interaction parameter where j = 0-2.

$$G^{\varphi} = y''_{Ge}G^{\varphi}_{Nb:Ge} + y''_{Si}G^{\varphi}_{Nb:Si} + 0.25RT(y''_{Ge}lny''_{Ge} + y''_{Si}lny''_{Si}) + y''_{Ge}y''_{Si}\sum {}^{j}L^{\varphi}_{Nb:Ge,Si}(y''_{Ge} - y''_{Si})^{j} \quad (6)$$

For Nb_3Ge, a two-sublattice model $(\mathbf{Nb})_{0.75}(\mathbf{Ge},Nb,Si)_{0.25}$ was used. The model for Nb_3Ge described by Geng et al. [10] placed a VA on the second sublattice. Based on assumption that VA substitution in the second sublattice is not thermodynamically favoured [8], the above model was used. The Gibbs energy function is given below, where φ = Nb_3Ge and ${}^{j}L$ is the interaction parameter for j = 0-2.

$$\begin{aligned} G^{\varphi} = {} & y''_{Ge}G^{\varphi}_{Nb:Ge} + y''_{Si}G^{\varphi}_{Nb:Si} + y''_{Nb}G^{\varphi}_{Nb:Nb} + 0.25RT(y''_{Ge}lny''_{Ge} + y''_{Si}lny''_{Si} + y''_{Nb}lny''_{Nb}) \\ & + y''_{Ge}y''_{Si}\sum {}^{j}L^{\varphi}_{Nb:Ge,Si}(y''_{Ge} - y''_{Si})^{j} + y''_{Ge}y''_{Nb}\sum {}^{j}L^{\varphi}_{Nb:Ge,Nb}(y''_{Ge} - y''_{Nb})^{j} \\ & + y''_{Nb}y''_{Si}\sum {}^{j}L^{\varphi}_{Nb:Nb,Si}(y''_{Nb} - y''_{Si})^{j} + y''_{Ge}y''_{Nb}y''_{Si}\sum {}^{0}L^{\varphi}_{Nb:Ge,Nb,Si} \end{aligned} \quad (7)$$

The model for αNb_5Si_3 is $(\mathbf{Nb},Si)_{0.625}(Ge,\mathbf{Si})_{0.375}$, based on the two sublattice model used by Geng et al. [9]. The Gibbs energy function is given below, where φ = αNb_5Si_3.

$$\begin{aligned} G^{\varphi} = {} & y'_{Nb}y''_{Ge}G^{\varphi}_{Nb:Ge} + y'_{Nb}y''_{Si}G^{\varphi}_{Nb:Si} + y'_{Si}y''_{Ge}G^{\varphi}_{Si:Ge} + y'_{Si}y''_{Si}G^{\varphi}_{Si:Si} \\ & + 0.625RT(y'_{Nb}lny'_{Nb} + y'_{Si}lny'_{Si}) + 0.375RT(y''_{Ge}lny''_{Ge} + y''_{Si}lny''_{Si}) \\ & + y'_{i}y''_{Ge}y''_{Si}\sum_{i=Nb,Si} {}^{j}L^{\varphi}_{i:Ge,Si}(y''_{Ge} - y''_{Si})^{j} + y''_{k}y'_{Nb}y'_{Si}\sum_{k=Ge,Si} {}^{j}L^{\varphi}_{Nb,Si:k}(y'_{Nb} - y'_{Si})^{j} \end{aligned} \quad (8)$$

Where y'_i and y''_k (i=Nb,Si and k=Ge,Si) is the site fraction of elements on the first or second sublattice sites respectively, a ${}^{j}L$ is the interaction parameter for j = 0-2.

The model for $Nb_5(Ge,Si)_3$ phase is a three-sublattice model $(Nb)_4(Ge,\mathbf{Nb},Si)_1(\mathbf{Ge},\mathbf{Si},VA)_3$. To account for solubility between βNb_5Si_3 and Nb_5Ge_3, mixing of Ge and Si on both second and third sublattice sites was permitted. The Gibbs energy function is given by the equation below, and φ = $Nb_5(Ge,Si)_3$.

$$
\begin{aligned}
G^{\varphi} = {} & y''_{Ge}y'''_{Ge}G^{\varphi}_{Nb:Ge:Ge} + y''_{Ge}y'''_{Si}G^{\varphi}_{Nb:Ge:Si} + y''_{Nb}y'''_{Ge}G^{\varphi}_{Nb:Nb:Ge} + y''_{Nb}y'''_{Si}G^{\varphi}_{Nb:Nb:Si} + y''_{Si}y'''_{Ge}G^{\varphi}_{Nb:Si:Ge} \\
& + y''_{Si}y'''_{Si}G^{\varphi}_{Nb:Si:Si} + y''_{Ge}y'''_{Va}G^{\varphi}_{Nb:Ge:Va} + y''_{Nb}y'''_{Va}G^{\varphi}_{Nb:Nb:Va} + y''_{Si}y'''_{Va}G^{\varphi}_{Nb:Si:Va} \\
& + 0.125RT(y''_{Ge}lny''_{Ge} + y''_{Nb}lny''_{Nb} + y''_{Si}lny''_{Si}) \\
& + 0.375RT(y'''_{Ge}lny'''_{Ge} + y'''_{Si}lny'''_{Si} + y'''_{Va}lny'''_{Va}) \\
& + \sum_{k=Ge,Si,Va} y''_{Ge}y''_{Si}y'''_{k} \sum {}^{j}L^{\varphi}_{Nb:Ge,Si:k}(y''_{Ge} - y''_{Si})^{j} \\
& + \sum_{k=Ge,Si,Va} y''_{Nb}y''_{Si}y'''_{k} \sum {}^{j}L^{\varphi}_{Nb:Nb,Si:k}(y''_{Nb} - y''_{Si})^{j} \\
& + \sum_{k=Ge,Si,Va} y''_{Ge}y''_{Nb}y'''_{k} \sum {}^{j}L^{\varphi}_{Nb:Ge,Nb:k}(y''_{Ge} - y''_{Nb})^{j} \\
& + \sum_{i=Ge,Nb,Si} y''_{i}y'''_{Ge}y'''_{Si} \sum {}^{j}L^{\varphi}_{Nb:i:Ge,Si}(y'''_{Ge} - y'''_{Si})^{j} \\
& + \sum_{i=Ge,Nb,Si} y''_{i}y'''_{Ge}y'''_{Va} \sum {}^{j}L^{\varphi}_{Nb:i:Ge,Va}(y'''_{Ge} - y'''_{Va})^{j} \\
& + \sum_{i=Ge,Nb,Si} y''_{i}y'''_{Si}y'''_{Va} \sum {}^{j}L^{\varphi}_{Nb:i:Si,Va}(y'''_{Si} - y'''_{Va})^{j}
\end{aligned}
$$

(9)

Where y''_i and y'''_k (i=Ge,Nb,Si and k=Ge,Si) are site fractions of elements in the second and third sublattice sites respectively, and ^{j}L is the interaction parameter where j = 0-2. Not all interaction parameters were required to sufficiently model the system, and were therefore set to zero.

The model for $CrSi_2$ prototype phases was taken from the description of $NbGe_2$ by Geng et al. [10]; **(**Ge,**Nb,Si**$)_{0.333}$(**Ge**,Nb,**Si**,$)_{0.667}$. The Gibbs energy function is given below, and φ =$CrSi_2$.

$$
\begin{aligned}
G^{\varphi} = {} & y'_{Nb}y''_{Si}G^{\varphi}_{Nb:Si} + y'_{Nb}y''_{Ge}G^{\varphi}_{Nb:Ge} + y'_{Nb}y''_{Nb}G^{\varphi}_{Nb:Nb} + y'_{Ge}y''_{Nb}G^{\varphi}_{Ge:Nb} + y'_{Ge}y''_{Si}G^{\varphi}_{Ge:Si} \\
& + y'_{Ge}y''_{Ge}G^{\varphi}_{Ge:Ge} + y'_{Si}y''_{Nb}G^{\varphi}_{Si:Nb} + y'_{Si}y''_{Si}G^{\varphi}_{Si:Si} \\
& + y'_{Si}y''_{Ge}G^{\varphi}_{Si:Ge}0.333RT(y'_{Ge}lny'_{Ge} + y'_{Nb}lny'_{Nb} + y'_{Si}lny'_{Si}) \\
& + 0.667RT(y''_{Ge}lny''_{Ge} + y''_{Nb}lny''_{Nb} + y''_{Si}lny''_{Si}) + \sum_{k=Ge,Nb,Si} y''_{k}y'_{Ge}y'_{Nb}\,{}^{0}L^{\varphi}_{Ge,Nb:k} \\
& + \sum_{k=Ge,Nb,Si} y''_{k}y'_{Ge}y'_{Si}\,{}^{0}L^{\varphi}_{Ge,Si:k} + \sum_{k=Ge,Nb,Si} y''_{k}y'_{Nb}y'_{Si}\,{}^{0}L^{\varphi}_{Nb,Si:k} \\
& + \sum_{i=Ge,Nb,Si} y'_{i}y''_{Nb}y''_{Si}\,{}^{0}L^{\varphi}_{i:Nb,Si} + \sum_{i=Ge,Nb.Si} y'_{i}y''_{Ge}y''_{Nb}\,{}^{0}L^{\varphi}_{i:Ge,Nb} \\
& + \sum_{i=Ge,Nb,Si} y'_{i}y''_{Ge}y''_{Si}\,{}^{0}L^{\varphi}_{i:Ge,Si}
\end{aligned}
$$

(10)

Where y'_i and y''_k (i=Ge,Nb,Si and k=Ge,Nb,Si) are site fractions of elements in the first or second sublattice sites respectively. Parameter values for $NbSi_2$ were taken directly from [9]. $NbGe_2$ was reoptimised here.

CALPHAD assessment was performed using the PARROT module in Thermocalc 2016b software. The Nb-Ge phase diagram was reassessed to make the enthalpy of formation values closer to ab initio results and to remove the inadvertent miscibility gap. In the ternary system, the complete solubility

between Nb_5Ge_3 and βNb_5Si_3 and limited solubility of Ge in αNb_5Si_3 were modelled first. The limited solubility of Si in Nb_3Ge and Ge in Nb_3Si were modelled subsequently. Where available, ab initio data from the literature were used for the metastable end members. The enthalpy of formation at 298 K was fixed as close to the calculated ab initio data as possible, whilst avoiding the appearance of the metastable phase in the binary diagram e.g. the enthalpy of formation for metastable Nb_5Ge_3 Cr_5Si_3-type must be less negative than Nb_5Ge_3 W_5Si_3-type which is the stable phase in Nb-Ge binary. Enthalpy of formation for stable and metastable end members from CALPHAD are compared to ab initio values in Table 2. Generally good agreement was achieved. Graphing of results was done using both Thermocalc 2016b and Pandat 8.2. Optimised values from the present work are given in Table 3.

6.0 Thermodynamic modelling results and discussion

6.1 Ge-Nb binary phase diagram

The reoptimised Ge-Nb phase diagram is shown in Figure 7a. The region around Nb_3Ge fits the experimental data of Jorda et al. well [25] (Fig. 7b-c) considering errors in the experimental data of ± 10°C for temperatures and ± 1 at. % for compositions. The miscibility gap has been removed. In Figure 8a the enthalpy of formation calculated using CALPHAD at 298 K is compared to the experimental data at 298 K [26-27] and ab initio data at 0 K [8]. The enthalpy of formation values are more negative compared to the previous assessment by Geng et al. [10], and are now closer to the ab initio values. In Figure 8b the calculated enthalpy of formation of the liquid at 1700 °C is compared to experimental data from Beloborodova [29] showing a good fit. This optimisation fits both the experimental [26-28] and ab initio enthalpy of formation data [8] generally well, considering the large reported error in the experimental data. For Nb_5Ge_3 an additional experimental point (solution calorimetry) is reported in the literature (-69.2 kJ/mol) [30] but is significantly different to the other experimental data and the ab initio calculations, and as such was not included in the optimisation. Compared to the 0 K ab initio values, the CALPHAD optimisation is less negative for Nb_5Ge_3 and $NbGe_2$. For Nb_3Ge, the opposite is true and the CALPHAD optimisation is more negative than the 0 K ab initio values.

It has been suggested in our previous publication [8], based on the ab initio calculations, that Nb_3Ge may in fact not be stable at low temperatures since the enthalpy of formation is above the ground state line between Nb and Nb_5Ge_3 (dashed line in Figure 8a). Further ab initio calculations showed that non stoichiometric Nb_3Ge crosses the ground state line at higher temperatures suggesting that it is a high temperature stable phase. However, to the authors knowledge there is no experimental data below approximately 900 K to confirm the stability of Nb_3Ge. Further experimental work is required to assess the phase diagram at lower temperatures. However, in the present paper, based on currently available data this is the best fit model.

6.2 Isothermal sections of Ge-Nb-Si

In Figs. 9a and 9b the calculated isothermal section for Ge-Nb-Si at 1820 °C is shown. Compared with the experimental data by Pan et al. [20, 21] (Fig. 4) the phase regions are well reproduced. In the current thermodynamic description, the Nb_5Si_3 phase identified by Pan et al. as the W_5Si_3 prototype (βNb_5Si_3), is instead identified as the Cr_5B_3 prototype (αNb_5Si_3). In the binary phase diagram both αNb_5Si_3 and βNb_5Si_3 are stable at 1820 °C (Fig. 1), and therefore both can appear in the ternary phase diagram. Therefore, the present thermodynamic description is a better representation of the ternary

system. Solubility of Ge in both phases creates a two phase region within the ternary phase diagram (Fig. 9a).

Nb_5Ge_3 and βNb_5Si_3 are modelled to have complete solid solubility. This region has some width given the solubility ranges of the two end member phases. In the diagrams by Pan et al. [20, 21], the $Nb_5(Si,Ge)_3$ region was drawn with width suggesting a Nb concentration that exceeded 62.5 at. %. This was not reproduced in the current model. In the binary phase diagrams for both Ge-Nb and Nb-Si the maximum Nb content for the W_5Si_3 prototype is 62.5 ± 1 at. %. As such this was maintained in the extrapolation to the ternary phase diagram.

Pan et al. [20, 21] give the composition of Nb_3Ge in the binary to be between approximately 16-18 at. % Ge at 1820 °C. Based on the currently accepted binary phase diagram (Fig. 7a) the homogeneity range of Nb_3Ge is between ~18-24 at. % Ge over the whole temperature range. The modelled Nb_3Ge single phase region reflects the binary phase region, but therefore does not correlate with all Pan et al.'s experimental data.

At 1780°C the calculated phase diagram (not shown) is similar to the isothermal section at 1820 °C. Pan et al. predicted that Nb_3Si should not be stable at 1780 °C. In the currently accepted Nb-Si phase diagram Nb_3Si is stable from 1977 °C down to 1673 °C (Fig. 1 [9]). Using the current model, the phase regions around Nb_3Si have been improved. In general, by taking into account more accurate binary phase diagram descriptions, improvements in the ternary phase diagram have been achieved.

In Figs. 10 and 11 the calculated isothermal sections at 1200 °C and 1500 °C are compared with the experimental data in the current study and the literature [7]. At 1200 and 1500 °C the diagram fits the data well along the pseudo binary between stoichiometric Nb_5Si_3 and Nb_5Ge_3.

Li et al. [7] made two alloys; ZF1 (Nb-18 Si- **5Ge**) and ZF2 (Nb-18Si-**10Ge**) heat treated at 1200 and 1500 °C. At 1200 °C, in ZF1 they identified three phases; αNb_5Si_3, Nb_{ss} and trace amounts of $Nb_5(Ge,Si)_3$ [7]. In our modelled phase diagram only two phases are predicted to form; αNb_5Si_3 and Nb_{ss}. At 1500 °C, they suggest that ZF1 is two-phase which agrees with the calculated diagram.

At 1200 °C in the alloy ZF2, αNb_5Si_3, $Nb_5(Ge,Si)_3$ and Nb_{ss} were identified in [7]. In calculated phase diagram ZF2 is just within the three-phase region containing αNb_5Si_3, Nb_{ss} and $Nb_5(Ge,Si)_3$. At 1500 °C they suggest that ZF2 is within a two-phase region, whereas the modelled phase diagram shows that the alloy should be well within a three-phase region. To fit the model to both the experimental data from [7] and the current study was not possible and hence the data in the current work was prioritised in the optimisation.

6.3 Nb_5Si_3-Nb_5Ge_3 isopleth

An isopeth at x(Nb)=0.625 was drawn and is shown in Figure 12. Since this diagram is drawn along a phase boundary, the tie-lines which intersect the boundary are also plotted, even though there will be zero amount of these phases present (e.g. BCC, Nb_3Si and Nb_3Ge are not stable phases along this phase boundary, but have tie-lines which intersect the boundary). As shown by the insets in Figure 12 there are thin phase regions between Liquid + $Nb_5(Ge,Si)_3$ and solid phase boundaries, and between $Nb_5(Ge,Si)_3$ + Nb_{ss}, and $Nb_5(Ge,Si)_3$ + Nb_3Ge and $Nb_5(Ge,Si)_3$ + Nb_3Si.

In this diagram the stability of the binary Nb_5Si_3 phases (low temperature stable αNb_5Si_3 and high temperature stable βNb_5Si_3) can be assessed when replacing Si with Ge, to understand the effect of Ge on phase stability. For example, at 1200 °C the modelling shows that $Nb_5(Ge,Si)_3$ is in equilibrium with αNb_5Si_3 when the Ge content exceeds 12.4 at. %. On the other hand, $Nb_5(Ge,Si)_3$ can be solely

stabilised (αNb_5Si_3 is not present) with additions in excess of 16.9 at. % Ge. The ternary phase diagrams (Fig. 10-11) however illustrate that away from stoichiometry, where Nb < 62.5 at. %, the amount of Ge required to stabilise $Nb_5(Ge,Si)_3$ is lower. A ternary phase region containing αNb_5Si_3, $Nb_5(Ge,Si)_3$ and $Nb(Ge,Si)_2$ is predicted to form at Nb < 62.5 at. % close to the Nb-Si binary phase region. At 1200 °C where Nb is 60 at. % and Ge+Si = 40 at. %, it is predicted that only 3.4 at. % Ge is needed to form $Nb_5(Ge,Si)_3$.

6.4 Liquidus projection

The liquidus projection (Fig. 13) shows 6 primary phase regions which are Nb_{ss}, $Nb_5(Ge,Si)_3$ $Nb(Ge,Si)_2$, Nb_3Si, Nb_3Ge and $(Ge,Si)_{ss}$. Two ternary invariant reactions are observed in the liquidus projection, indicated in Fig. 13 as (i) and (ii), and are listed in Table 4. The primary solidification regions calculated were compared with the data from [7] along with the Scheil solidification curves calculated for ZF1 (Nb-18Si-**5Ge**) and ZF2 (Nb-18Si-**10Ge**) (Fig. 14). For the alloys ZF1 and ZF2, the formation of primary $Nb_5(Ge,Si)_3$ was reported [7]. In the micrographs this is surrounded by Nb_{ss} and a fine eutectic which the authors report contains $Nb_5(Ge,Si)_3$ and Nb_{ss}. For ZF2, the modelled liquidus projection and Scheil solidification curve agrees with this solidification path. However the model suggests that a ternary eutectic containing Nb_3Si, Nb_{ss} and $Nb_5(Ge,Si)_3$ will form instead of a binary eutectic. The suggested solidification path for ZF2 is: $L \rightarrow L + Nb_5(Ge,Si)_3 \rightarrow L+Nb_5(Ge,Si)_3 + Nb_{ss} \rightarrow Nb_5(Ge,Si)_3 + Nb_{ss} + [Nb_5(Ge,Si)_3 + Nb_{ss} + Nb_3Si]_{eutectic}$. For ZF1, the solidification path calculated is slightly different. The primary phase is again $Nb_5(Ge,Si)_3$, but following this Nb_3Si forms before the eutectic. A ternary eutectic again occurs. The suggested solidification path for ZF1 is: $L \rightarrow L + Nb_5(Ge,Si)_3 \rightarrow L + Nb_3Si \rightarrow L+Nb_3Si + Nb_{ss} \rightarrow Nb_5(Ge,Si)_3 +Nb_3Si + Nb_{ss} + [Nb_5(Ge,Si)_3 + Nb_{ss} + Nb_3Si]_{eutectic}$.

Although Nb_3Si was not identified in [7], the phase may be present in the alloys ZF1 and ZF2. The fine eutectic formed, overlapping XRD peaks and similar contrast in backscattered SEM would make it difficult to distinguish this phase. Tweddle [31] gives evidence for the presence of Nb_3Si from the eutectic. In a complex multi component alloy containing Nb, Ti, Si, Cr, Al, Ge and Y, Nb_3Si could not be resolved initially in the as-cast microstructure using XRD or SEM/EDX. After heat treatment at 1300°C - 1500°C for 100 h under Ar, Nb_3Si was observed in the microstructure adjacent to βNb_5Si_3, where previously a eutectic microstructure had been seen. Pure Nb_3Si is not stable at 1300°C - 1500°C, however titanium substitution will stabilise the phase to lower temperatures [32] and allow growth of this phase as the eutectic coarsens during heat treatment.

7.0 Conclusions

A thermodynamic dataset has been developed to describe the Ge-Nb-Si system using the CALPHAD method. The Ge-Nb binary system was reoptimised to fit recent ab initio data for the enthalpy of formation of the intermetallic phases and to remove a small inadvertent miscibility gap in a previous optimisation. Ternary thermodynamic models were extrapolated from the binary phase diagram descriptions and fitted to experimental data reported in the present paper, along the Nb_5Si_3- Nb_5Ge_3 pseudo binary, and data from the literature. For stoichiometric 5:3 phases complete solid solubility exists between βNb_5Si_3 and Nb_5Ge_3 (both of which have the W_5Si_3 prototype) above 1934 °C, referred to as $Nb_5(Ge,Si)_3$. Below 1934 °C αNb_5Si_3 is stable, forming a two-phase region containing αNb_5Si_3 and $Nb_5(Ge,Si)_3$. Stoichiometric βNb_5Si_3 is not stable below 1934°C. But replacing Si with Ge stabilises the W_5Si_3 prototype to lower temperatures. For example, at 1200 °C $Nb_5(Ge,Si)_3$ will form when Ge content exceeds 12.4 at. %. In non-stoichiometric $Nb_5(Ge,Si)_3$, where Nb < 62.5 at. %, lower amounts of Ge are required to stabilised the W_5Si_3 prototype e.g. 3.4 at. % at 1200 °C.

Other phases also extend into the ternary phase diagram. $NbGe_2$ and $NbSi_2$ and both Si and Ge exhibit complete solid solubility. Nb_3Ge and Nb_3Si have limited solubility, up to 2 at. % Si and 6 at. %

Ge respectively. The sublattice models for Nb_3Ge was modified to remove vacancy substitution giving the current model $(Nb)_3(\mathbf{Ge},Nb,Si)_1$.

The current model fits well with the previously published phase diagram at 1820 °C, as well as the data reported in the present paper. Improvements to the description of the phase diagrams from the literature have been made by taking into account more recent binary phase diagram descriptions for Nb-Si and Ge-Nb binary phase diagrams, and experimental data presented in the current work, to provide a self-consistent description for the ternary phase diagram.

Acknowledgements

The authors would like to thank Rolls-Royce Plc and EPSRC (EP/ H500405/1 and EP/L026678/1) for funding and Dr Nathalie Dupin (Calcul Thermodynamique) and Dr Andrew Watson (University of Leeds) for helpful discussion.

Appendix A. Supplementary data – Ge-Nb-Si thermodynamic database

References

[1] P. Tsakiropoulos, Beyond Nickel Based Superalloys. In: R. B, W. S, (Eds.). Encyclopedia of Aerospace Engineering: John Wiley & Sons, Ltd, 2010.
[2] M.R. Jackson, B.P. Bewlay, J.C. Zhao. vol. US patent 6913655 B2, July 5, 2005.
[3] Cockeram BV, Rapp RA. Oxidation-resistant boron- and germanium-doped silicide coatings for refractory metals at high temperature, Mater. Sci. Eng. A 192/193 (1995) 980e6.
[4] M.R. Jackson, B.P. Bewlay, J.C. Zhao. vol. US patent 6419765, July 16, 2002.
[5] L. Su, L. Jia, J. Weng, Z. Hong, C. Zhou, H. Zhang, Improvement in the oxidation resistance of Nb–Ti–Si–Cr–Al–Hf alloys containing alloyed Ge and B, Corrosion Science 88 (2014) 460–465.
[6] E.S.K. Menon, M.G. Mendiratta, D.M. Dimiduk, Oxidation behavior of complex niobium based alloys, Proceedings of the International Symposium Niobium 2001, Orlando, FL, USA, 121-145.
[7] Z. Li, P. Tsakiropoulos, Study of the effects of Ge addition on the microstructure of Nb-18Si in situ composites, Intermetallics 18(2010) 1072-1078.
[8] I. Papadimitriou, C. Utton, P. Tsakiropoulos, On the Nb-Ge binary system, Metall. Mater. Trans. A 46 (2015) 5526-5536.
[9] T. Geng, C. Li, X. Zhao, H. Xu, Z. Du, C. Guo, Thermodynamic assessment of the Nb-Si-Mo system, Calphad 34 (2010) 363-376.
[10] T. Geng, C.R. Li, Z.M. Du, C.P. Guo, X.Q. Zhao, H.B. Xu, Thermodynamic assessment of the Nb-Ge system, J. Alloys Compd. 509 (2011) 3080-3088.
[11] H. Okamoto, Ge-Nb (Germanium-Niobium), J. Phase Equilib. Diffus. 33 (2012) 250-251.
[12] H. Nowotny, A.W. Searcy, J.E. Orr. Structures of some germanides of formula M_5Ge_3, J. Phys. Chem. 60 (1956) 677-678.
[13] J.L. Jorda. Phase-diagram of system Nb-Ge, Helvetica Physica Acta 51 (1978) 455.
[14] V.M. Pan, O.G. Kulik, V.I. Latysheva. Silicon influence on phase-composition and critical-temperature of superconducting Niobium-Germanium alloys, Fizika Metallov I Metallovedenie 47 (1979) 1114-1117.
[15] C. Colinet, J. Tedenac, Enthalpies of formation of TM–X compounds (X=Al, Ga,Si,Ge,Sn). Comparison of ab-initio values and experimental data, CALPHAD 54 (2016) 16-34.
[16] V.M. Pan, V.I. Latysheva, O.G. Kulik, A.G. Popov, and L.E.N. Izuvestiya: Russian Metallurgy, Translated from Izvestiya Akademii Nauk SSSR., Metally, 1982, vol. 3, p. 167.
[17] K.W. Richter, H. Flandorfer, H.F. Franzen. On the stability of hexagonal Ge_7Nb_{10}, Journal of Alloys and Compounds 320 (2001) 87-92.
[18] M. Kloska, E.L. Haase. On the existence of the hexagonal Nb_3Ge_2 phase, Journal of the Less Common Metals 99 (1984) 241-248.
[19] SGTE Solutions Database Version 4.8 (SSOL4)
[20] V.M. Pan, V.I. Latysheva, O.G. Kulik, A.G. Popov, Influence of alloying with germanium and copper on the conditions of formation of the superconducting compound Nb_3Si, Russ. Metall. 3 (1982) 167-171.

[21] V.M. Pan, V.I. Latysheva, O.G. Kulik, A.G. Popov, Influence of mutual alloying on the formation and superconductivity of Nb_3Ge and Nb_3Si, Russ. Metall. 4 (1982) 167-169.
[22] L.H. Brixner, X-ray study and thermoelectric properties of $NbSi_xGe_{2-x}$ and the $TaSi_xGe_{2-x}$ systems, J. Inorg. Nucl. Chem. 25 (1961) 257-260.
[23] A.T. Dinsdale, STGE data for pure elements, Calphad 15(4) (1991) 317-425.
[24] M. Hillert, L.I. Staffansson, The Regular Solution Model for Stoichiometric Phases and Ionic Melts, Acta Chem. Scand. 24 (1970) 3618-3626.
[25] J.L. Jorda, R. Flukiger, J. Muller, The phase diagram of the niobium-germanium system, J. Less-common Met. 63 (1978) 25–37.
[26] J.H. Carpenter, The composition range, decomposition pressure, and thermodynamic stability of Nb_3Ge, Journal of Physical Chemistry 67 (1963) 2141–2144.
[27] J.H. Carpenter, A.W. Searcy, The decomposition pressures of α- and β-Nb_5Ge_3 and the thermodynamic stability of $NbGe_2$, Journal of Physical Chemistry 67 (1963) 2144–2147.
[28] F.R. deBoer, R. Boom, W.C.M. Mattens, A.R. Miedema, A.K. Niessen, Cohesion in Metals. Transition Metal Alloys, 1988 (North-Holland, Amsterdam, Netherlands).
[29] E.A. Beloborodova, Poroshkovaya Metallurgiya, 7–8 (1996), pp. 76–79 (in Russian)
[30] W.-G.Jung, O.J.Kleppa, Standard molar enthalpies of formation of Me_5Ge_3 (Me=Zr, Nb, Mo), MeGe (Me=Ru, Rh,Pd) and Pd_2Ge by high-temperature calorimetry, J. Less-Common Met. 169 (1991) 93–103.
[31] A. Tweddle, Study of the effect of Ge and Y additions on the microstructure, phase stability and environmental degradation of Nb silicide alloys, PhD thesis, University of Sheffield 2015.
[32] H. Liang, Y.A. Chang, Thermodynamic modelling of the Nb-Si-Ti ternary system, Intermetallics 7 (1999) 561-570.

Table 1: Nominal compositions in atomic fraction for Ge-Nb-Si samples

Sample	Nb	Si	Ge
5 at. % Ge	0.625	0.325	0.05
10 at. % Ge	0.625	0.275	0.10
15 at. % Ge	0.625	0.225	0.15
20 at. % Ge	0.625	0.175	0.20
30 at. % Ge	0.625	0.075	0.30

Table 2: Enthalpy of formation data for binary end member phases presently assessed using Calphad compared with first principles calculation [8]. Phase in bold is a stable end member.

Structure	Phase	Enthalpy of formation, kJ/mol	
		ab initio, 0 K	Calphad, 298 K
*tI*32 Cr_5B_3	Nb_5Ge_3	-46.53	-42
	Nb_5Si_3	**-61.2**	**-63.001**
*tI*32 W_5Si_3	**Nb_5Ge_3**	**-46.63**	**-42.892**
	Nb_5Si_3	-58.2	-50.636
*tP*32 Ti_3P	Nb_3Ge	-30.213	-25
	Nb_3Si	**-37.3**	**-33.357**
*cP*8 Cr_3Si	**Nb_3Ge**	**-29.387**	**-26.41**
	Nb_3Si	-34.73	-32
*hP*9 $CrSi_2$	**$NbGe_2$**	**-37.87**	**-33.24**
	$NbSi_2$	**-49.9**	**-51.2**

Table 3: Optimised parameters for phases in Ge-Nb and Ge-Nb-Si systems from the present work. Full database is given in supplementary information.

Phase name	Sublattice model and parameters		Ref.
	GHSERGE =-9486.153+165.635573 T-29.5337682 T LN(T) +.005568297 T^2-1.513694E-06 T^3+163298 $T^{(-1)}$	298.15<T<900 K	
	= -5689.239+102.86087 T-19.8536239 T LN(T)-.003672527 T^2	900<T<1211.4 K	
	= -9548.204+156.708024 T-27.6144 T LN(T)-8.59809E+28 $T^{(-9)}$	1211.4<T<3200 K	
	GHSERNB= -8519.353+142.045475 T-26.4711 T LN(T) +2.03475E-04 T^2 -3.5012E-07 T^3+93399 $T^{(-1)}$	298.15<T<2750 K	
	= -37669.3+271.720843 T-41.77 T LN(T) + 1.528238E+32 $T^{(-9)}$	2750<T<6000 K	
	GHSERSI=-8162.609+137.236859 T-22.8317533 T LN(T) -.001912904 T^2-3.552E-09 T^3+176667 $T^{(-1)}$	298.15<T<1687 K	
	= -9457.642+167.281367 T-27.196 T LN(T)-4.20369E+30 $T^{(-9)}$	1687<T<3600 K	
Liquid	Model (Ge,Nb,Si)		
	$^0L^{Liquid}_{Ge,Nb} = -181600 + 9.309T$		a
	$^1L^{Liquid}_{Ge,Nb} = +71573 - 26.753T$		a
	$^2L^{Liquid}_{Ge,Nb} = +107936 - 42.037T$		a
	$^3L^{Liquid}_{Ge,Nb} = -42706 + 10.004T$		a
	$^0L^{Liquid}_{Ge,Si} = +6610 - 0.354T$		[19]
	$^0L^{Liquid}_{Nb,Si} = -199000$		[9]
	$^1L^{Liquid}_{Nb,Si} = -18800$		[9]
	$^2L^{Liquid}_{Nb,Si} = +50000$		[9]
BCC	Model (Ge,Nb,Si)(VA)$_3$		
	$^0L^{BCC}_{Ge,Nb} = -169559 + 17.328\,T$		a
	$^0L^{BCC}_{Nb,Si} = -151178$		[9]
	$^1L^{BCC}_{Nb,Si} = -15915$		[9]
	$^2L^{BCC}_{Nb,Si} = +40000$		[9]
Diamond	Model (Ge,Nb,Si)		
	$^0L^{Diamond}_{Ge,Nb} = -85000 - 2T$		a
	$^0L^{Diamond}_{Ge,Si} = +3500$		[19]
Nb_3Ge	Model (Nb)$_{0.75}$(Ge,Nb,Si)$_{0.25}$		
	$G^{Nb_3Ge}_{Nb:Ge} = 0.75$ GHSERNB $+ 0.25$ GHSERGE $- 26410 - 7.386T$		a
	$G^{Nb_3Ge}_{Nb:Nb} =$ GHSERNB $+ 43850 - 2.565$T		a
	$G^{Nb_3Ge}_{Nb:Si} = 0.75\ GHSERNB + 0.25\ GHSERSI - 32000 + 4.04879T$		a
	$^0L^{Nb_3Ge}_{Nb:Ge,Nb} = -80989 + 7.443T$		a
	$^1L^{Nb_3Ge}_{Nb:Ge,Nb} = -30118 + 31.536T$		a
	$^0L^{Nb_3Ge}_{Nb:Ge,Si} = -21841$		a
	$^0L^{Nb_3Ge}_{Nb:Ge,Nb,Si} = -93588$		a
Nb_3Si	Model (Nb)$_{0.75}$(Ge,Si)$_{0.25}$		
	$G^{Nb_3Si}_{Nb:Si} = 0.75\ GSHERNB + 0.25\ GSHERSI - 33357 - 6.45T$		[9]
	$G^{Nb_3Si}_{Nb:Ge} = 0.75\ GSHERNB + 0.25\ GHSERGE - 25000 + 18.75T$		a
	$^0L^{Nb_3Si}_{Nb:Ge,Si} = -57960$		a
αNb_5Si_3	Model (Nb,Si)$_{0.625}$(Ge,Si)$_{0.375}$		
	$G^{Nb_5Si_3}_{Nb:Si} = 0.625\ GHSERNB + 0.375\ GHSERSI - 63001.35 - 2.9T$		[9]
	$G^{Nb_5Si_3}_{Nb:Ge} = 0.625\ GHSERNB + 0.375\ GHSERGE - 42000 - 6.74477T$		a
	$G^{Nb_5Si_3}_{Si:Ge} = 0.625\ GHSERSI + 0.375\ GHSERGE + 5000$		a
	$G^{Nb_5Si_3}_{Si:Si} = GHSERSI + 5000$		a
	$^0L^{Nb_5Si_3}_{Nb,Si:Si} = -12226$		[9]
	$^0L^{Nb_5Si_3}_{Nb:Ge,Si} = -43202 + 16.555T$		a
	$^1L^{Nb_5Si_3}_{Nb:Ge,Si} = -15205 + 3.2631T$		a
$Nb_5(Ge,Si)_3$	Model (Nb)$_{0.5}$(Ge,Nb,Si)$_{0.125}$(Ge,Si,VA)$_{0.375}$		
	$G^{Nb_5(Ge,Si)_3}_{Nb:Nb:Si} = 0.625\ GHSERNB + 0.375\ GHSERSI - 50636.5 - 8.5T$		[9]
	$G^{Nb_5(Ge,Si)_3}_{Nb:Nb:Ge} = 0.625\ GHSERNB + 0.375 GHSERGE - 42892 - 8.101T$		a
	$G^{Nb_5(Ge,Si)_3}_{Nb:Si:Si} = 0.5\ GHSERNB + 0.5\ GHSERSI - 18312 - 15.2836T$		[9]

	$G^{Nb_5(Ge,Si)_3}_{Nb:Ge:Ge} = 0.5\ GHSERNB + 0.5\ GHSERGE - 6112.7 - 14.947T$	a
	$G^{Nb_5(Ge,Si)_3}_{Nb:Ge:Si} = 0.5\ GHSERNB + 0.125\ GHSERGE + 0.375\ GHSERSI - 50000$	a
	$G^{Nb_5(Ge,Si)_3}_{Nb:Si:Ge} = 0.5\ GHSERNB + 0.125\ GHSERSI + 0.375\ GHSERGE - 47202$	a
	$G^{Nb_5(Ge,Si)_3}_{Nb:Si:VA} = 0.5\ GHSERNB + 0.125\ GHSERSI + 5000$	a
	$G^{Nb_5(Ge,Si)_3}_{Nb:Ge:VA} = 0.5\ GHSERNB + 0.125\ GHSERGE - 14747 - 1.603T$	a
	$G^{Nb_5(Ge,Si)_3}_{Nb:Nb:VA} = 0.625\ GHSERNB + 55000$	a
	${}^0L^{Nb_5(Ge,Si)_3}_{Nb:Nb,Si:Si} = -24318$	a
	${}^0L^{Nb_5(Ge,Si)_3}_{Nb:Ge,Nb:*} = -34357 + 2.606T$	a
	${}^0L^{Nb_5(Ge,Si)_3}_{Nb:\#:Ge,VA} = -8591.6 - 1.001T$	a
	${}^0L^{Nb_5(Ge,Si)_3}_{Nb:Ge,Nb:Si} = -35000$	a
	${}^0L^{Nb_5(Ge,Si)_3}_{Nb:Nb,Si:Ge} = 0$	a
	${}^0L^{Nb_5(Ge,Si)_3}_{Nb:Nb:Ge,Si} = -66408 + 29.180T$	a
	${}^1L^{Nb_5(Ge,Si)_3}_{Nb:Nb:Ge,Si} = -5653.6$	a
$Nb(Ge,Si)_2$	Model $(Ge,Nb,Si)_{0.333}(Ge,Nb,Si)_{0.667}$	
	$G^{Nb(Ge,Si)_2}_{Ge:Ge} = GHSERGE + 18624 + 4.833T$	a
	$G^{Nb(Ge,Si)_2}_{Ge:Nb} = 0.333\ GHSERGE + 0.667\ GHSERNB - 5376 + 3.051T$	a
	$G^{Nb(Ge,Si)_2}_{Si:Ge} = 0.333\ GHSERSI + 0.667\ GHSERGE + 5000$	[9]
	$G^{Nb(Ge,Si)_2}_{Si:Nb} = 0.333\ GHSERSI + 0.667\ GHSERNB + 5000$	a
	$G^{Nb(Ge,Si)_2}_{Si:Si} = GHSERSI + 5000$	[9]
	$G^{Nb(Ge,Si)_2}_{Nb:Ge} = 0.333\ GHSERNB + 0.667\ GHSERGE - 33240 - 12.115T$	a
	$G^{Nb(Ge,Si)_2}_{Nb:Nb} = GHSERNB + 29496 - 7.953T$	a
	$G^{Nb(Ge,Si)_2}_{Nb:Si} = 0.333\ GHSERNB + 0.667\ GHSERSI - 51200 - 5.0T$	[9]
	${}^0L^{Nb(Ge,Si)_2}_{Ge,Nb:\#} = -19200 + 7T$	a
	${}^0L^{Nb(Ge,Si)_2}_{\#:Ge,Nb} = -81400 + 30T$	a
	${}^0L^{Nb(Ge,Si)_2}_{Nb,Si:Si} = +12919 + 4.2662T$	[9]
	${}^0L^{Nb(Ge,Si)_2}_{Nb:Ge,Si} = -7000$	a

a = value from present work, * Ge or VA, # Nb or Ge

Table 4: Ternary Invariant reactions

T, °C	**Invariant Reaction**	**x(GE)**	**x(NB)**	**x(SI)**
1921	Liquid -> Nb_{ss} + $Nb_5(Ge,Si)_3$ + Nb_3Ge	0.123	0.800	0.077
1907	Liquid -> Nb_{ss} + $Nb_5(Ge,Si)_3$ + Nb_3Si	0.050	0.809	0.141

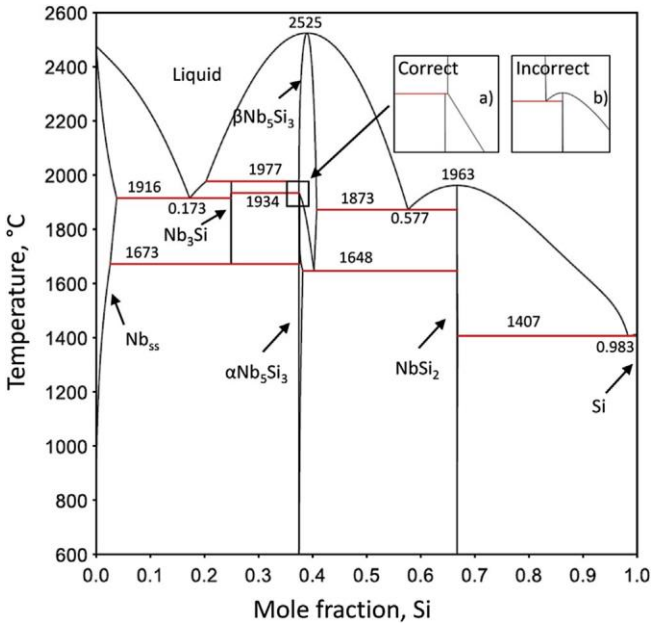

Fig. 1. Nb-Si calculated binary phase diagram as described by Geng et al. [9].

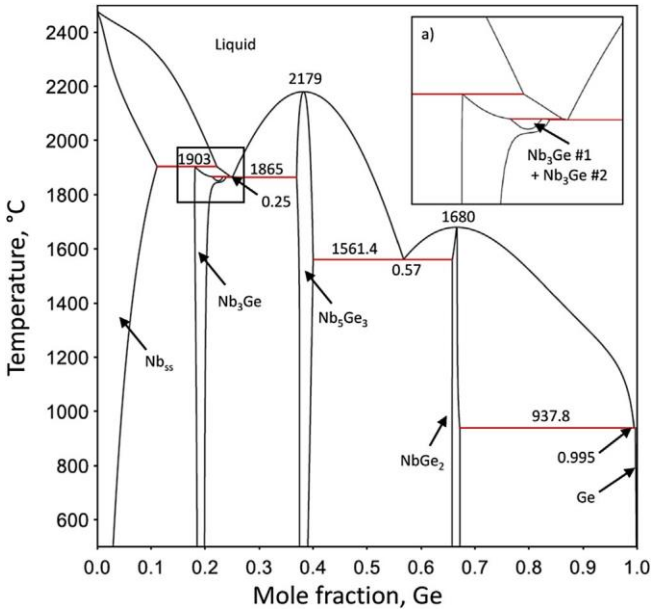

Fig. 2. Ge-Nb calculated binary phase diagram as described in Geng et al. [10].

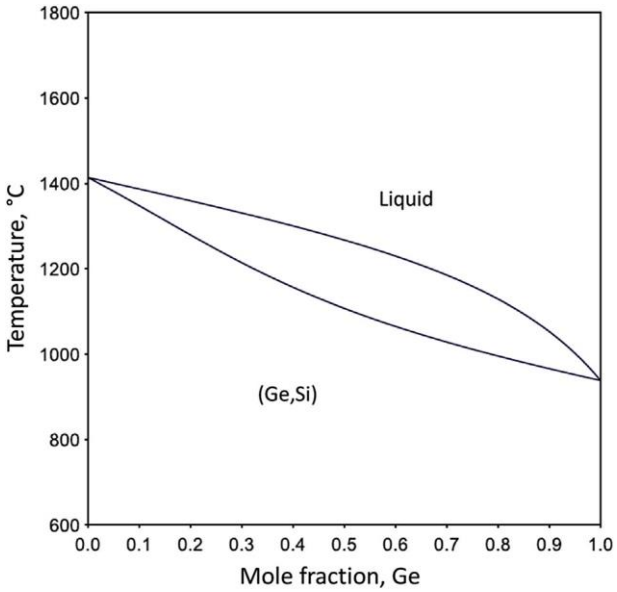

Fig. 3. Ge-Si calculated binary phase diagram as described by SGTE Alloy Solutions Database v4.9 g.

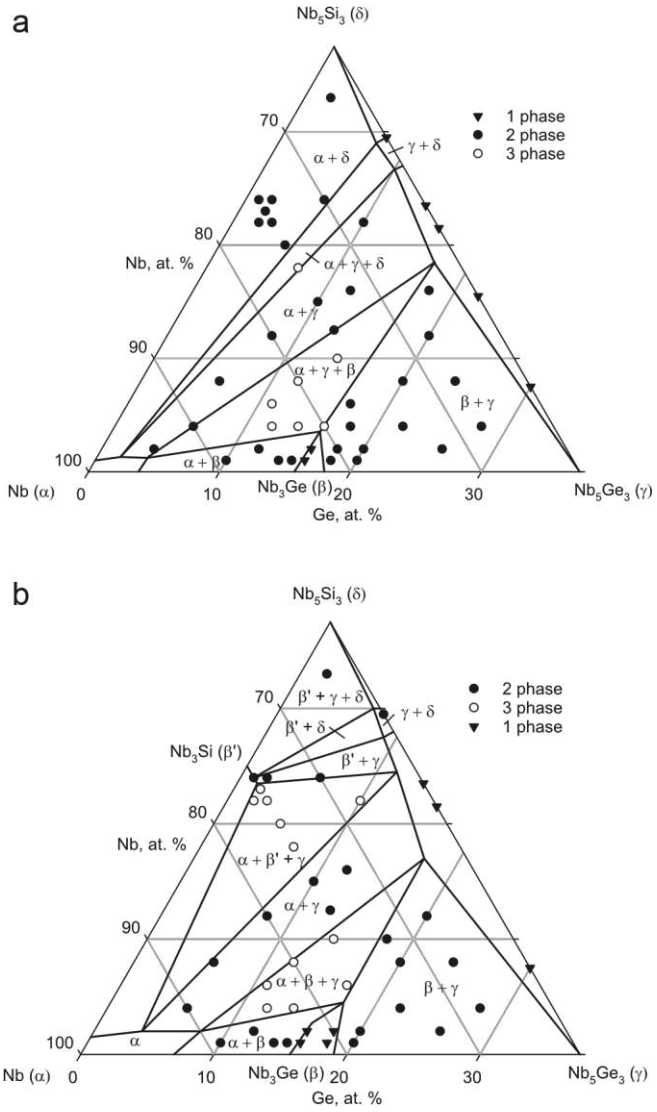

Fig. 4. Ge-Nb-Si isothermal sections at a) 1780 °C (2053K) and b) 1820 °C (2093K). The diagrams have been redrawn based on original hand drawn images by Pan et al. [20,21]. Key - open circle is a three phase region, filled circle is a two phase region, triangle is a single phase region. Phases are referred to as α - Nb, β - Nb_3Ge, β' - Nb_3Si, δ - Nb_5Si_3, γ - Nb_5Ge_3 in Refs. [20,21].

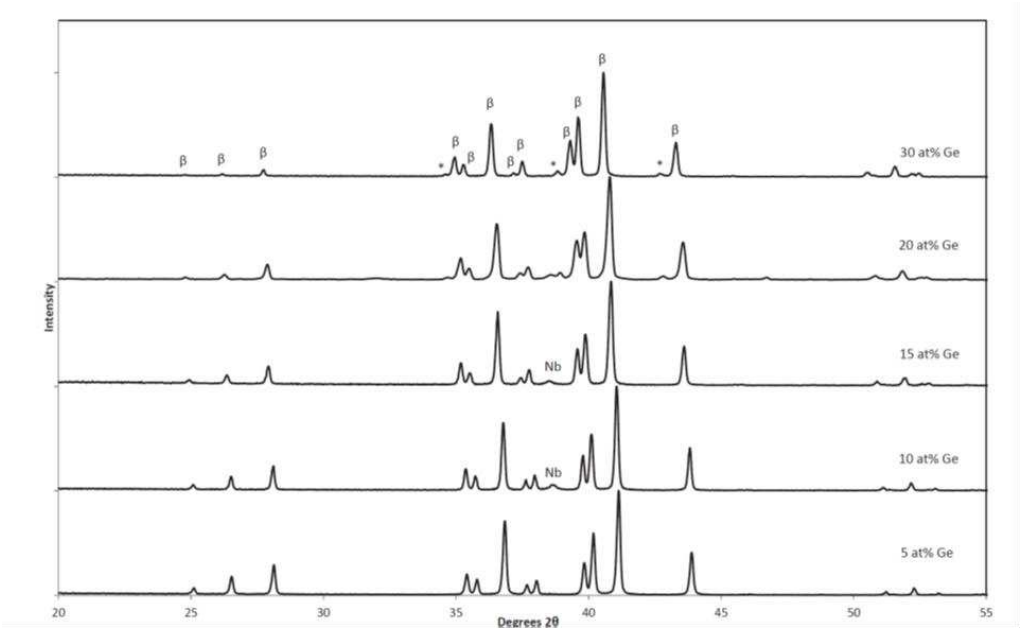

Fig. 5. XRD of As-Cast samples with 5, 10, 15, 20 and 30 at. % Ge. Key: β - $Nb_5(Ge,Si)_3$, Nb - Nb_{ss}, * - Nb_3Ge

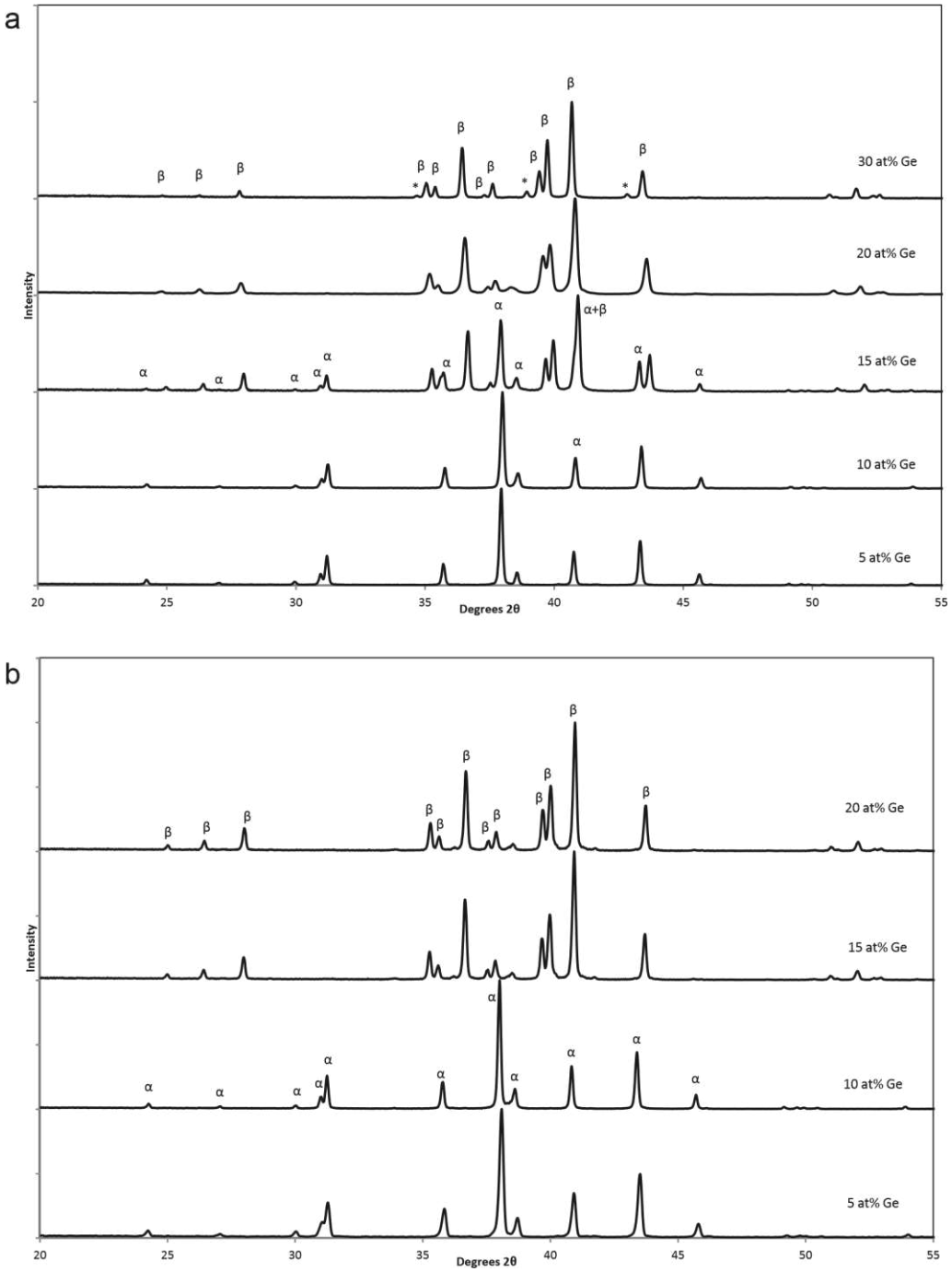

Fig. 6. XRD of samples heat treated at a) 1200 and b) 1500 C with 5, 10, 15, 20 and 30 at. % Ge. Key: β - $Nb_5(Ge,Si)_3$, α - Nb_5Si_3.

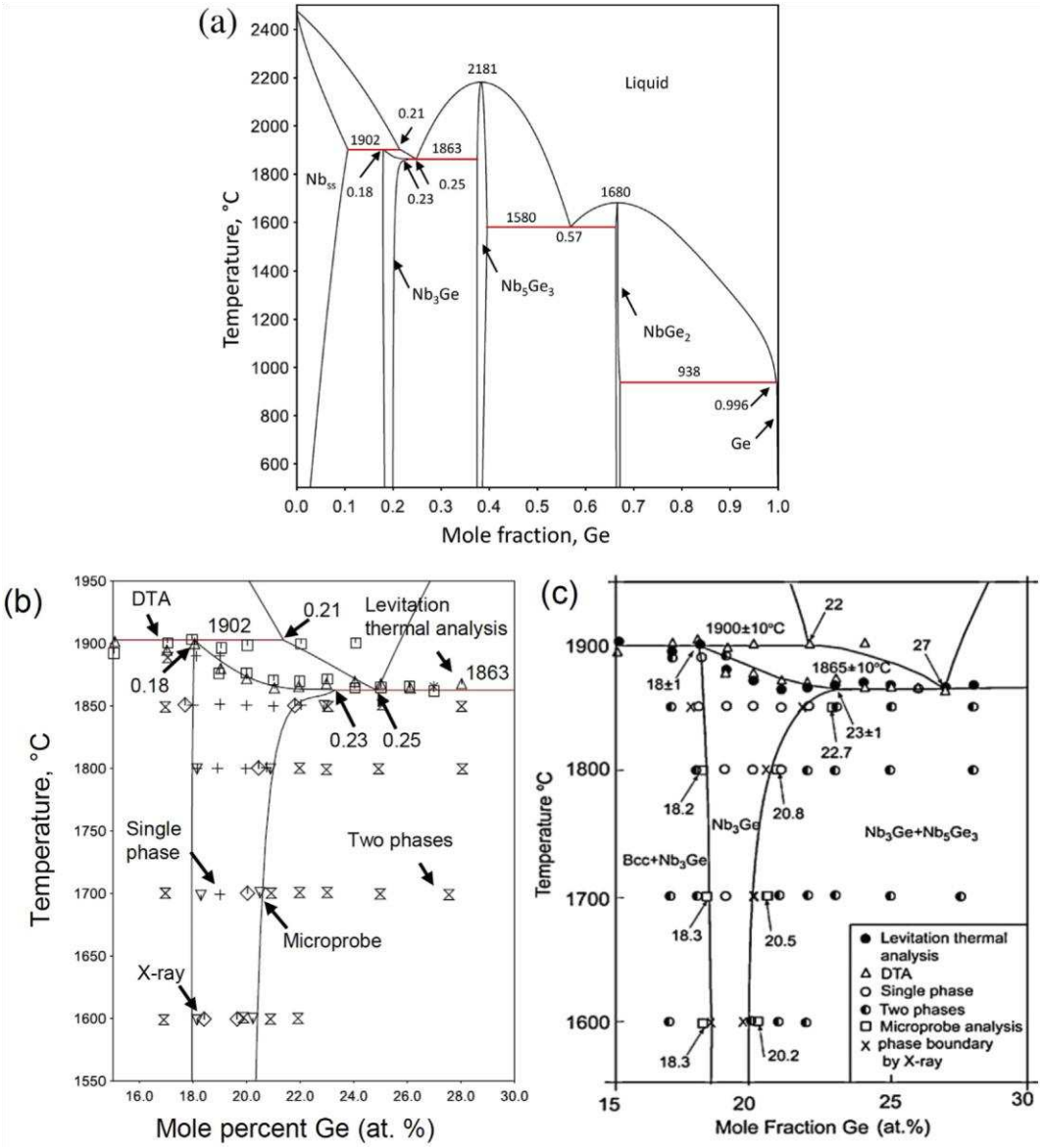

Fig. 7. a) Reoptimised Ge-Nb binary phase diagram b) Nb_3Ge region compared to data from Jorda et al. [25] and c) experimental phase diagram evaluated by Jorda et al. [25].

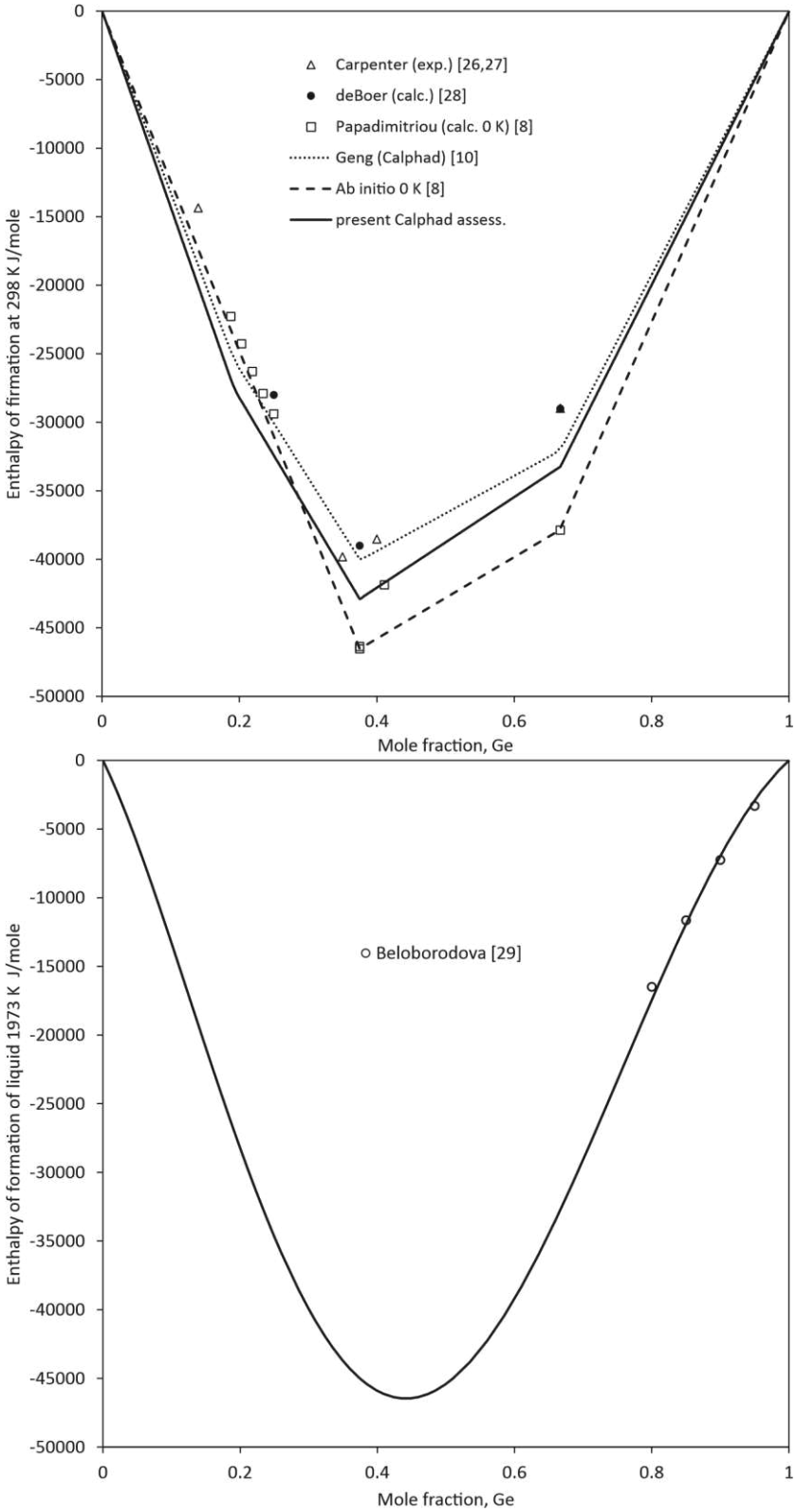

Fig. 8. a) Enthalpy of formation for the Nb-Ge system at 25 °C compared with the experimental data at 25 C [26-28] and ab initio data at 0 K [8] and b) enthalpy of formation of the liquid at 1700 °C compared to experimental data from Beloborodova [29]. Reference states are liquid Nb and liquid Ge.

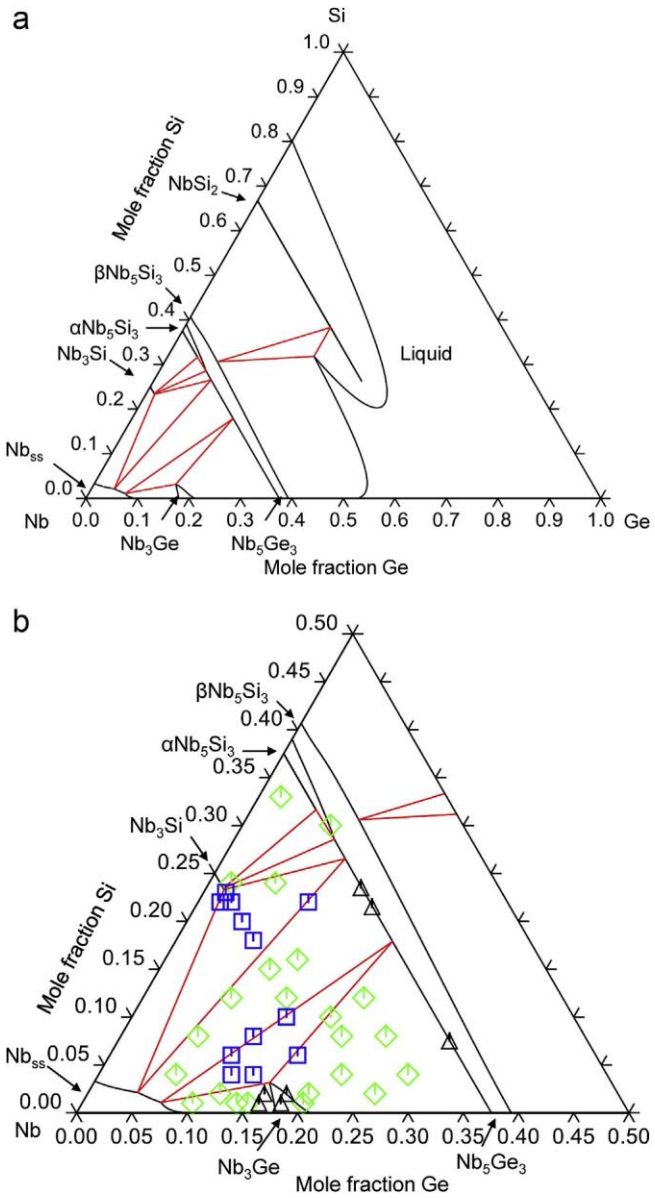

Fig. 9. a) Ge-Nb-Si isothermal section at 1820 °C b) Nb-rich region of Ge-Nb-Si isothermal section at 1820 °C, compared with data from Pan et al. [20,21]. Key: Triangle - single phase region, diamond - two-phase region, square - three-phase region.

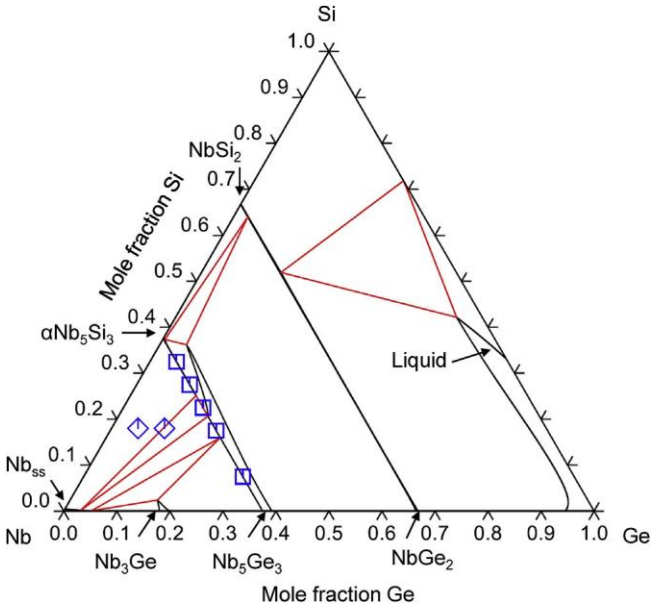

Fig. 10. Ge-Nb-Si isothermal section at 1200 °C (1473 K) compared to data in the current study (squares) and [7] (diamonds).

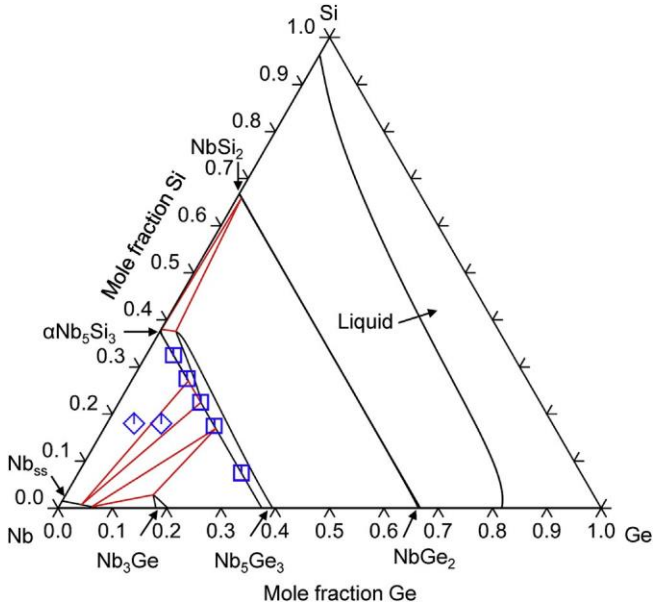

Fig. 11. Ge-Nb-Si isothermal section at 1500 °C (1773 K) compared to data in the current study (squares) and [7] (diamonds).

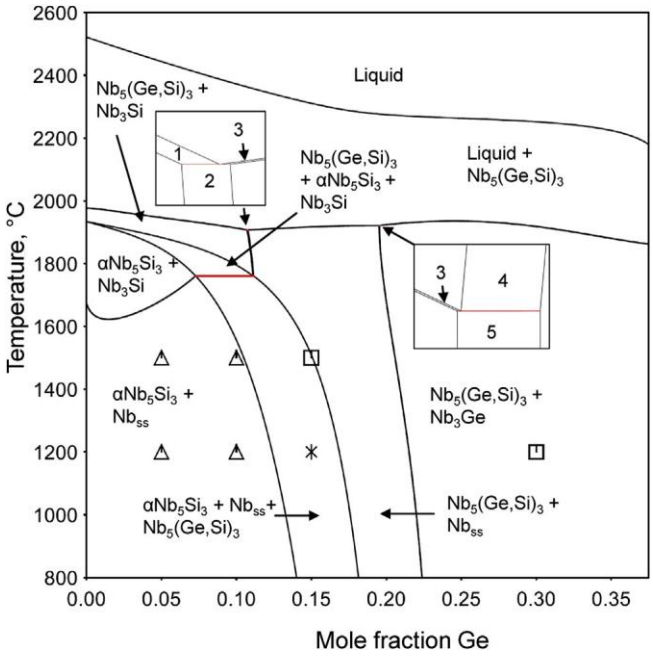

Fig. 12. Isopleth section at x(Nb) = 0.625 with experimental data from current work. Key: triangle - α-Nb_5Si_3, star - α-Nb_5Si_3 + β-Nb_5Si_3, square - β-Nb_5Si_3. Insets show thin phase regions. Numbers refer to phase regions: 1: L + Nb_3Si + $Nb_5(Ge,Si)_3$, 2: Nb_{ss} + Nb_3Si + $Nb_5(Ge,Si)_3$, 3: L + Nb_{ss} + $Nb_5(Ge,Si)_3$, 4: L + Nb_3Ge + $Nb_5(Ge,Si)_3$, 5: Nb_{ss} + Nb_3Ge + $Nb_5(Ge,Si)_3$

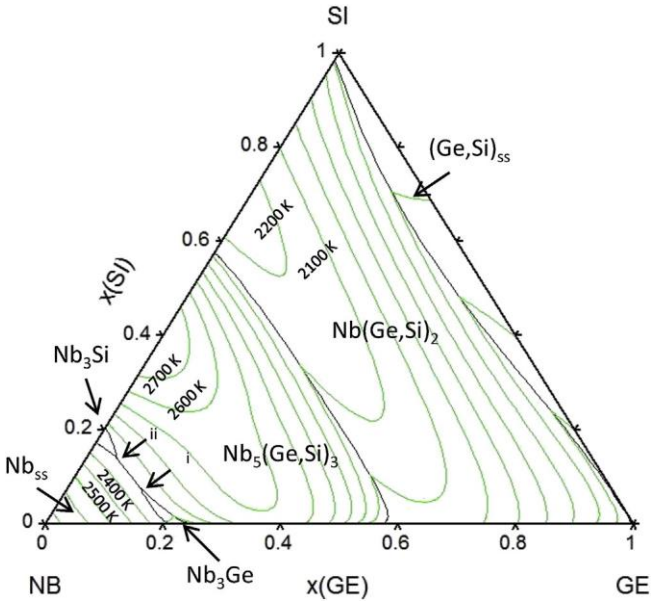

Fig. 13. Liquidus projection for Ge-Nb-Si with isothermal lines every 100 K

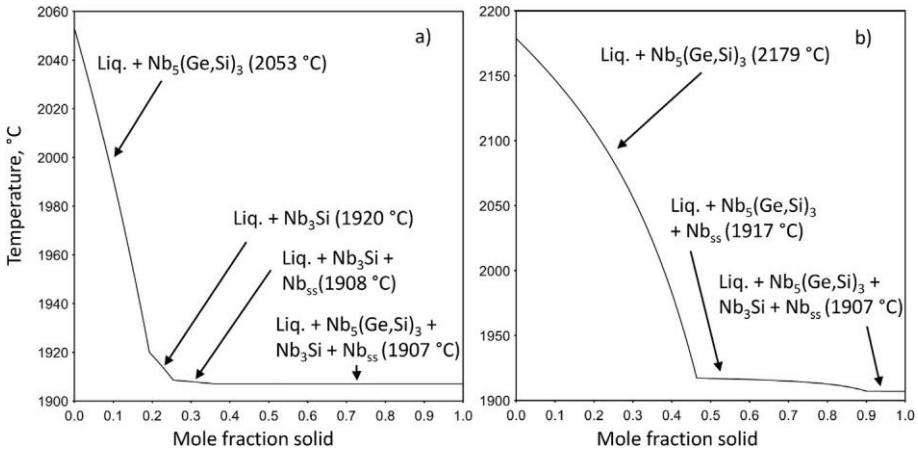

Fig. 14. Scheil solidification curves for ternary alloys a) Nb-18Si-5Ge b) Nb-18Si-10Ge.